Inorg. Chem. **2005**, *44*, 9405–9415

Chromate Nanorods/Nanobelts: General Synthesis, Characterization, and Properties

Jiahe Liang,[†] Qing Peng,[†] Xun Wang,[†] Xi Zheng,[†] Ruji Wang,[†] Xinping Qiu,[†] Cewen Nan,[‡] and Yadong Li*[,†,§]

Department of Chemistry and the Key Laboratory of Atomic & Molecular Nanosciences (Ministry of Education, China), Tsinghua University, Beijing 100084, P. R. China, National Center for Nanoscience and Nanotechnology, Beijing 100084, P. R. China, and Department of Materials Science and Engineering, Tsinghua University, Beijing 100084, P. R. China

Received December 15, 2004

A general synthesis route to a family of single-crystal chromate nanorods/nanobelts has been established. The effects of pH and surfactant on phase and morphology of these microcrystalline materials have been investigated. The physical properties of the as-synthesized chromate nanocrystals such as dielectric, electrochemical, UV–vis absorbance, and photoluminescent properties have also been studied. The present general synthesis of various low-dimensional chromate nanomaterials provides useful information on the possible synthesis of other microcrystalline transition metal oxysalts.

Introduction

"General synthesis", which is also regarded as "systematic synthesis", is a synthetic method to produce a family of specific compounds with similar structures or properties via a similar approach.[1] More rules of the synthetic conditions and more scientific information of the compounds can be provided in the "general synthesis" method, which is more helpful for us to improve the synthetic science. Hence, general synthesis of the family of related materials is a very interesting direction for synthesis methodology and material science.[2]

Transition metal oxysalts of chromate comprise a very important family of inorganic materials that have potential applications in many fields such as photosensitizers and photoconductive dielectric materials,[3] effective solid lubricants,[4] very promising interconnecting materials for solid oxide fuel cell (SOFCs),[5] tunable near-infrared lasers,[6] catalysts in many organic reactions,[7] ionic conductors because of their thermal stability and electrical properties,[8] and magnetic materials.[9] Due to their unique properties and applications in many fields, the preparation of such transition metal oxysalts of chromate in the nanosize range has attracted much attention recently. Previous synthetic approaches include solid-state reaction,[10] Langmuir−Blodgett (L−B) techniques,[11] reverse micelles and microemulsion methods,[12] pyrolysis techniques,[13] template-directing methods by using the surfactant of polymer,[14] and hydrothermal methods.[15] However, while individual compounds of chromate can be

* To whom correspondence should be addressed. E-mail: ydli@tsinghua.edu.cn.

[†] Department of Chemistry and the Key Laboratory of Atomic & Molecular Nanosciences (Ministry of Education, China), Tsinghua University.

[‡] Department of Materials Science and Engineering, Tsinghua University.

[§] National Center for Nanoscience and Nanotechnology.

(1) (a) Suh, S.; Hoffman, D. M. *J. Am. Chem. Soc.* **2000**, *122*, 9396−9404. (b) Duan, X. F.; Liber, C. M. *Adv. Mater.* **2000**, *12*, 298−302.
(2) (a) O'Brien, S.; Brus, L.; Murray, C. B. *J. Am. Chem. Soc.* **2001**, *123*, 12085−12086. (b) Takayama, Y.; Delas, C.; Muraoka, K.; Uemura, M.; Sato, F. *J. Am. Chem. Soc.* **2003**, *125*, 14163−14167.
(3) Liang, J. H.; Li, Y. D. *J. Cryst. Growth*, **2004**, *261*, 577−580.
(4) Ouyang, J. H.; Sasaki, S.; Umeda, K. *Surf. Coat. Technol.* **2002**, *154*, 131−139.
(5) Sakai, N. *Ceramics* **1995**, *30*, 329 (in Japanese).
(6) Aoki, Y.; Konno, H. *J. Solid State Chem.* **2001**, *156*, 370−378.
(7) (a) Ahn, B. T.; Park, H. S.; Lee, E. J.; Um, I. H. *B Kor. Chem. Soc.* **2000**, *21*, 905−908. (b) Adkins, H. In *Organic Reactions*; Adams, R., Ed.; Wiley: New York, 1954; Vol. 8, p 1.
(8) (a) Saavedra, M. J.; Parada, C.; Rojo, J. M. *J. Mater. Chem.* **1998**, *8*, 2077−2080. (b) Leon, C.; Lucia, M. L.; Santamaria, J. *Philos. Mag. B* **1997**, *75*, 629−638.
(9) (a) Aoki, Y.; Konno, H. *J. Mater. Chem.* **2001**, *11*, 1458−1464. (b) Bueno, I.; Parada, C.; Saez, R.; Baran, E. J. *J. Alloys Compd.* **1995**, *225*, 237−241.
(10) Knight, K. S. *Mineral. Mag.* **2000**, *64*, 291−300.
(11) Yang, P. D.; Kim, F. *ChemPhysChem* **2002**, *3*, 503.
(12) (a) Shi, H. T.; Qi, L. M.; Ma, J. M.; Cheng, H. M.; Zhu, B. Y. *Adv. Mater.* **2003**, *15*, 1647. (b) Panda, A. K.; Bhowmik, B. B.; Das, A. R.; Moulik, S. P. *Langmuir* **2001**, *17*, 1811−1816. (c) Li, M.; Schnablegger, H.; Mann, S. *Nature* **1999**, *402*, 393−395.
(13) Aoki, Y.; Konno, H. *J. Mater. Chem.* **2001**, *11*, 1458−1464.
(14) Yu, S. H.; Colfen, H.; Antonietti, M. *Chem.—Eur. J.* **2002**, *8*, 2937−2945.

10.1021/ic048237+ CCC: $30.25
Published on Web 11/01/2005

successfully synthesized via the above methods, to the best of our knowledge, there are few reports on the general synthesis of the family of chromates up to now.

Herein, we report a general procedure and characterization of a family of single-crystal chromate nanorods/nanobelts by hydrothermal treatment. The reaction conditions such as the effect of pH and surfactant have been investigated, and the rules of the general synthesis have been summarized. Moreover, some physical properties of the as-synthesized chromate nanocrystals, such as dielectric, electrochemical, UV−vis absorbance, and photoluminescent characteristics, have also been studied.

Experimental Section

Synthesis Materials. Analytical grade chemicals of $K_2Cr_2O_7$, NaOH, $Pb(Ac)_2$, $CuCl_2 \cdot 2H_2O$, $CaCl_2$, $SrCl_2$, $Ba(NO_3)_2$, $Zn(NO_3)_4 \cdot 6H_2O$, $Ni(Ac)_2$, and $AgNO_3$ and the surfactants of PVP (average MW: 1 300 000), PEG (average polymerization degree: 400), PVA (average polymerization degree: 1750 ± 50), stearylamine, stearinic acid, CTAB (cetyltrimethylammonium bromide), and SDS (sodium dodecyl sulfate) were purchased from Beijing Chemical Reagent Co. and used without further purification.

Synthesis Method. In a typical procedure, $K_2Cr_2O_7$ solution (10 mL, 0.1 M) was mixed with $Pb(Ac)_2$, $CuCl_2 \cdot 2H_2O$, $CaCl_2$, $SrCl_2$, $Zn(NO_3)_4 \cdot 6H_2O$, $Ni(Ac)_2$, $Ba(NO_3)_2$, or $AgNO_3$ solution (20 mL, 0.1 M) in a 50-mL capacity Teflon-lined stainless autoclave and stirred by using a glass rod at room temperature. The pH of the mixture was adjusted to a specific value by adding NaOH solution (1.0 M) or diluted nitric acid (1:1). The autoclave was sealed and maintained at 140 °C for 20 h and then allowed to cool naturedly. The products were filtered off, washed three times with deionized water and absolute ethanol, and dried at 60 °C for 6 h in air. In the presence of surfactants, about 1 wt % of PVP, PEG, PVA, stearylamine, stearinic acid, CTAB, and SDS was added to the mixtures prior to the adjustment of pH value.

The reaction was carried out in a 50-mL capacity Teflon-lined stainless autoclave in a digital-type temperature-controlled oven.

Measurements of Properties. XRD, SEM, TEM, HRTEM, PL spectroscopy, and an impedance analyzer were used to characterize the products. Powder X-ray diffraction (XRD) was carried out by using a Brucker D8-Advance X-ray diffractometer with Cu Kα radiation ($\lambda = 1.5418$ Å) using a 40 kV operation voltage and 40 mA current. SEM was operated using a LEO-1530 scanning electron microscopy (SEM) with an accelerating voltage of 20 kV. The sample was sprayed with Au prior to the measurement with SEM to enhance the conductivity. Transmission electron microscopy (TEM) and high-resolution TEM (HRTEM) were performed on a Hitachi model H-800 transmission electron microscope and a JEOL-2010F field emission transmission electron microscope, respectively. The accelerating voltages are all 200 kV.

The samples for dielectric measurement were pressed into a disk shape pellet of 9.34 mm in diameter and 1.23 mm thickness at a pressure of 10 MPa using poly(vinyl alcohol) as the binder. The pellets were finally sintered at a low temperature of 200 °C for 2 h in air. Sintered samples were polished, and electrodes were made by painting silver paste on both sides of the disk-shaped samples. The dielectric behavior was measured with an impedance analyzer (model HP4194A, Hewlett Packard, Palo Alto, CA) in the frequency ranges 100 Hz−40 MHz at a bias voltage of 1.0 V.

The electrochemical properties of $PbCrO_4$ nanorods were investigated by means of electrochemical insertion and extraction of Li ions into or from $PbCrO_4$ nanorods using a button-type cell with a Li-metal counter electrode serving as a Li-ion source. The working electrodes were composed of $PbCrO_4$, carbon black, and poly(vinylidene fluoride) at a weight ratio of 80:14:6. The mixed slurry was uniformly cast on an aluminum foil, dried at 110 °C for 24 h, and rolling-pressed. The cells were assembled with Cellgard 2300 as the separator and 1 M $LiPF_6$ in dimethyl carbonate (DMC) and ethylene carbonate (EC) (1:1 v/v) as the electrolyte. All cells were assembled and sealed in an argon-flled glovebox and tested on a Neware charge−discharge cycler at room temperature.

Optical diffuse reflectance of the samples was recorded on Shimadzu UV-2100S spectrophotometer. PL spectra were obtained with a Hitachi F-4500 fluorescence spectrophotometer at room temperature.

Results and Discussion

General Synthesis of Chromate Nanorods/Nanobelts. A family of chromate nanorods/nanobelts with high crystallinity is produced via a hydrothermal process at 140 °C for 20 h in the presence of surfactant of PVP (poly(vinyl pyrrolidone)) (1 wt %). The pH value of the parent mixture is found to be important for the formation of chromate nanorods/nanobelts in the reaction, and the optimal pH is about equal to 7.

Both nanorods and nanobelts could be classified as one-dimensional nanostructures. The difference between nanorods and nanobelts, on the basis of the electron microscopic results, is that (1) the cross sections of lots of nanorods are round-like shapes and the cross sections of a great number of nanobelts are rectangle-like shapes and (2) the aspect ratio of nanobelts is usually (not all) bigger than that of nanorods.

The general formula for the formation of chromate nanostructures can be described in eqs 1 and 2:

$$M(II) + Cr_2O_7^{2-} \xrightarrow[140°C,20h,PVP]{pH=7} \begin{cases} \xrightarrow{\text{nanorods}} MCrO_4\downarrow \ (M=Pb,Ba,Sr,Ni,Zn) \\ \xrightarrow{\text{nanobelts}} MCrO_4\downarrow \ (M=Cu,Ca,Sr) \end{cases} \quad (1)$$

$$2M(I) + Cr_2O_7^{2-} \xrightarrow[140°C,20h,PVP]{pH=7} M_2CrO_4\downarrow \ (M=Ag) \quad (2)$$

It should be illustrated that the chemical formula of Zn-based chromate in eq 1 is $4ZnCrO_4 \cdot K_2O \cdot 3H_2O$, which is different from the common formula of $MCrO_4$, and nanorod and nanobelt structures coexist in the sample of Sr-based chromate. In addition, the morphology of as-synthesized Ag-based chromate, shown in eq 2, includes both particle and rodlike structures.

Lead, strontium, zinc, and copper chromates have been chosen to be the examples for this study. Typical X-ray diffraction (XRD) patterns of chromate nanorod/nanobelt structures are shown in Figure 1. All the reflections in Figure 1a−c can be readily indexed to the pure monoclinic phase

(15) (a) Zheng, W.; Pang, W.; Meng, G.; Peng, D. *J. Mater. Chem.* **1999**, *9*, 2833−2836. (b) Sviridov, V. V.; Shevchenko, G. P.; Afanaseva, Z. M.; Ponyavina, A. N.; Loginova, N. V. *Colloid J.* **1996**, *58*, 372−376.

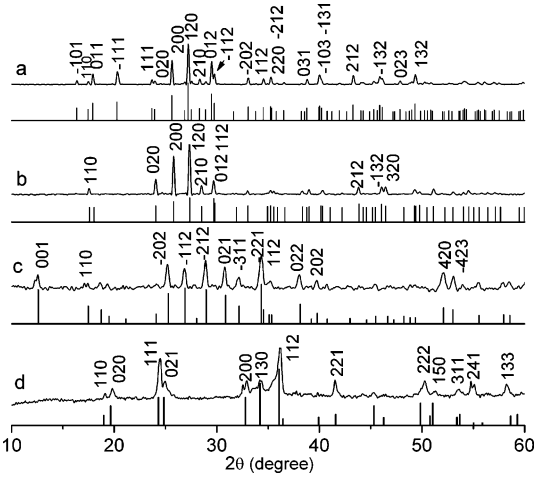

Figure 1. XRD patterns of as-synthesized chromate nanostructures: (a) $PbCrO_4$ nanorods; (b) $SrCrO_4$ nanorods; (c) $4ZnCrO_4{\cdot}K_2O{\cdot}3H_2O$ nanorods; (d) $CuCrO_4$ nanobelts. All the products are obtained at 140 °C for 20 h in the presence of surfactant PVP, pH 7. The histogram, just below the XRD pattern, shows the calculated powder diffraction pattern arising from (a) JCPDS 73-2059, (b) JCPDS 35-0743, (c) JCPDS 8-0202, and (d) JCPDS 34-0507, respectively.

(space group $P2_1/n$ (No. 14)) of $PbCrO_4$ with lattice constants $a = 7.12$ Å, $b = 7.43$ Å, $c = 6.79$ Å, and $\beta = 102.420°$ (JCPDS: 73-2059), $SrCrO_4$ with lattice constants $a = 7.09$ Å, $b = 7.39$ Å, $c = 6.76$ Å, and $\beta = 103.20°$ (JCPDS: 35-0743), and $4ZnCrO_4{\cdot}K_2O{\cdot}3H_2O$ with lattice constants $a = 9.277$ Å, $b = 6.363$ Å, $c = 7.745$ Å, and $\beta = 114.90°$ (JCPDS: 8-0202). Figure 1d shows the XRD pattern of $CuCrO_4$. The reflection peaks of this sample are in good agreement with an orthorhombic type structure (space group *Cmcm* (No. 63)), with lattice constants $a = 5.457$ Å, $b = 9.025$ Å, $c = 5.882$ Å, and $\alpha = \beta = \gamma = 90°$ (JCPDS: 34−0507). It is obvious that the chemical composition is $MCrO_4$ except that Zn-based chromate is $4ZnCrO_4{\cdot}K_2O{\cdot}3H_2O$ (the formula is also described as $K_2Zn_4O(CrO_4)_4{\cdot}3H_2O$), which is not consistent with the common formula.

The typical images of scanning electron microscopy (SEM) and transmission electron microscopy (TEM) of the as-synthesized products of $PbCrO_4$ nanorods and $CuCrO_4$ nanobelts are shown in Figure 2. As shown in Figure 2a,b, the morphology of as-synthesized $PbCrO_4$ is rodlike, which is highly uniform with diameters 60−80 nm and lengths up to 1.5 μm. The selected area electron diffraction (SAED) pattern (inset in Figure 2b) taken from a single nanorod reveals the single-crystalline nature of the sample. The high-resolution TEM image (Figure 2c) demonstrates that the nanorods are structurally uniform and the interplanar spacing of nanorods is about 5.4 Å corresponding to the $(\bar{1}01)$ plane. In addition, the HRTEM (high-resolution TEM) also confirms that the nanorods of $PbCrO_4$ are straight and perfect over their entire lengths.

The size and morphology of $CuCrO_4$ nanobelts is shown in Figure 2d−f. As shown in Figure 2d,e, the morphology of $CuCrO_4$ is beltlike structure, with the widths about average 30−40 nm, the thicknesses about average 29 nm, and lengths up to tens of micrometers. It is also observed that the belt structure is highly continuous and uniform. The SAED pattern (the inset in Figure 2e) is also taken on a single nanobelt. The regularly arranged spots in it reveal the single-crystalline nature of the as-prepared sample of $CuCrO_4$. The HRTEM image of the $CuCrO_4$ sample is exhibited in Figure

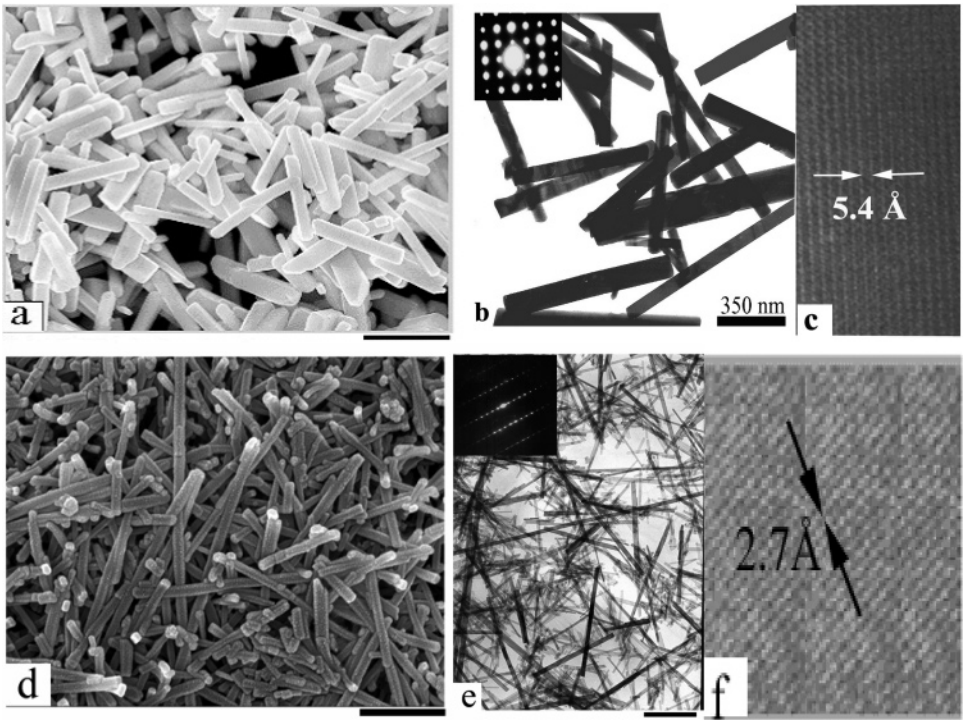

Figure 2. Typical electron microscopic images of $PbCrO_4$ nanorods and $CuCrO_4$ nanobelts: (a) SEM image of $PbCrO_4$ (bar = 1 μm); (b) TEM image of $PbCrO_4$ (inset shows the SAED pattern); (c) HRTEM image of $PbCrO_4$;[3] (d) SEM image of $CuCrO_4$ (bar = 0.5 μm); (e) TEM image of $CuCrO_4$ (inset shows the SAED pattern, bar = 0.5 μm); (f) HRTEM image of $CuCrO_4$. To enhance the conductivity, the samples were sprayed with Au powder prior to being detected with SEM.

Table 1. Summary of Related Parameters of a Family of Chromate Nanostructures

inorg precursor	phase	crystalline type	morphology	diameter/width (nm)	max length (μm)	av aspect ratio
$Pb(Ac)_2 + K_2Cr_2O_7$	$PbCrO_4$	monoclinic	nanorods	60−80	1.5	6.4
$CuCl_2 \cdot 2H_2O + K_2Cr_2O_7$	$CuCrO_4$	orthorhombic	nanobelts	30−40	20	26.3
$CaCl_2 + K_2Cr_2O_7$[a]	$CaCrO_4$	body-centered tetragonal	nanobelts	50−80	1.25	10.6
$SrCl_2 + K_2Cr_2O_7$	$SrCrO_4$	monoclinic	nanorods/nanobelts	30−60	1.6	22.7/8.7
$Ba(NO_3)_2 + K_2Cr_2O_7$	$BaCrO_4$	orthorhombic	nanorods	30−65	1.8	8.6
$Zn(NO_3)_4 \cdot 6H_2O + K_2Cr_2O_7$	$4ZnCrO_4 \cdot K_2O \cdot 3H_2O$	monoclinic	nanorods	40−60	1.6	9.4
$Ni(Ac)_2 + K_2Cr_2O_7$	$NiCrO_4$	orthorhombic	nanorods/particles	50−70	1.2	7.3
$AgNO_3 + K_2Cr_2O_7$	Ag_2CrO_4	orthorhombic	nanorods/particles	60−70	1.6	6.5

[a] $CaCl_2$ solution should be a saturated or concentrated solution, and ethanol is an indispensable solvent for the formation of $CaCrO_4$.

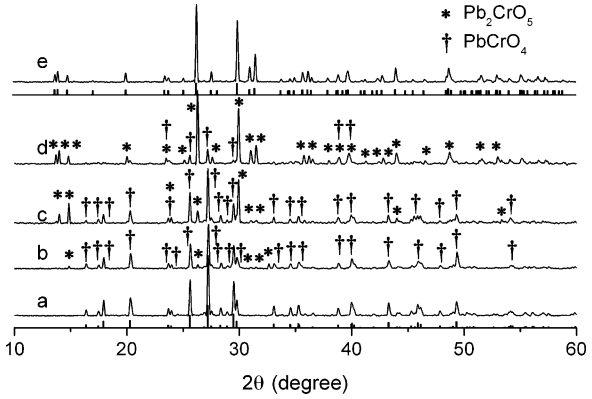

Figure 3. XRD patterns of Pb-based chromate products synthesized at 140 °C for 20 h in the absence of surfactant: (a) pH 1; (b) pH 4; (c) pH 7; (d) pH 9; (e) pH 14. An asterisk indicates the pure phase of $PbCrO_4$, and a dagger indicates the pure phase of Pb_2CrO_5. The reflections of (a) are in good agreement with the pure $PbCrO_4$ standard reflections of JCPDS 73-2059, and the reflections of (e) are well consistent with the pure Pb_2CrO_5 standard reflections of JCPDS 84-0678. The histogram, just below the XRD pattern, shows the calculated powder diffraction pattern arising from (a) JCPDS 73-2059 and (e) JCPDS 84-0678, respectively. On the basis of eq 3, the phase content of $PbCrO_4$ is (a) 100%, (b) 95.9%, (c) 66%, (d) 18.1%, and (e) 0, respectively.

2f, and the interplanar spacing is about 2.7 Å, which corresponds to the (200) plane.

The other chromate 1D nanostructures such as $BaCrO_4$, $SrCrO_4$, $CaCrO_4$, $NiCrO_4$, $4ZnCrO_4 \cdot K_2O \cdot 3H_2O$, and Ag_2CrO_4 nanorods/nanobelts have also been fabricated successfully using the current hydrothermal method. The related parameters of as-synthesized products are summarized in Table 1. (XRD patterns and TEM images of some other chromates are shown in the Supporting Information.)

Effect of pH on the Formation of Chromate Nanorods/Nanobelts. The initial pH of the precursor medium has a vital effect on both the formation of the chromate phase and its size and shape in the present synthetic process. Controlled experiments have been carried out to investigate the influence of pH on the morphology formation of chromates, as well as phase evolution.

Effect of pH on the Synthesis of Pb-Based Chromate Nanorods. Initial pH of solution has an effect on the formation of Pb-based chromate nanostructures. As detected by the XRD patterns in Figure 3, the pure $PbCrO_4$ sample can be produced under initial pH 1 (JCPDS: 73-2059) (Figure 3a). The morphology of the sample is described as spherical-like particles (Figure 4a). In the solution of pH 1, $Cr_2O_7^{2-}$ ions are dominant in the solution. The reason for the formation of $PbCrO_4$ is the extremely small solubility product constant of $PbCrO_4$ ($k_{sp} = 1.8 \times 10^{-14}$). When the pH is increased to 4, the products are mainly composed of $PbCrO_4$ phases with a few impurities of Pb_2CrO_5 phases (Figure 3b). It is interesting that the morphology of the prepared products is mainly that of rodlike structures although there contains some particle-like and planklike structures, which indicates that the morphology evolution from particle-like structure to rodlike structure occurs with the increasing pH. While the solution pH is increased to 7, the morphology of the sample consists of rodlike structures and the particle-like structures vanish, which further confirms the morphology evolution from particles to rods (Figure 4c). It is also seen in Figure 4c that there are some downy tubelike structures coexisting with rodlike structures. The representative downy tubelike structure is covered with the white panes referred to as I and II, and the enlarged image of I is shown in Figure 4d. Although there are varied viewpoints for the compositions of the downy tubes,[16] the rodlike structure might be $PbCrO_4$ on the basis of three reasons: (i) As shown in the XRD pattern of Figure 3c, the products synthesized at pH 7 contain two phases of $PbCrO_4$ and Pb_2CrO_5, and the dominant phase is $PbCrO_4$. Accordingly, the dominant morphology in Figure 4c should be the rodlike structure. (ii) The phase content of $PbCrO_4$ is estimated by using the following equation:[17]

$$X_{PbCrO_4} = [I(200)_{PbCrO_4} + I(120)_{PbCrO_4} + I(012)_{PbCrO_4}]/[I(200)_{PbCrO_4} + I(120)_{PbCrO_4} + I(012)_{PbCrO_4} + I(310)_{Pb_2CrO_5} + I(\bar{1}12/\bar{4}20)_{Pb_2CrO_5}] \quad (3)$$

Here, $I(200)_{PbCrO_4}$, $I(210)_{PbCrO_4}$, $I(012)_{PbCrO_4}$, $I(310)_{Pb_2CrO_5}$, and $I(\bar{1}12/\bar{4}20)_{Pb_2CrO_5}$ are the integrated intensities of the corresponding reflections. The result of the above equation is approximately 66%. (iii) The SAED pattern taking on a single solid rodlike structure is completely consistent with the standard reflections of $PbCrO_4$ nanorods. With further increase of the initial pH of the solution to 9, the dominant phase of the product becomes Pb_2CrO_5 instead of $PbCrO_4$ (Figure 3d). It is shown that the phase contents of Pb_2CrO_5 increase and $PbCrO_4$ decrease with the increment of pH. The morphology of the corresponding sample is shown in Figure 4e. Both rods and particles can be seen in Figure 4e, and morphology percentage is smaller than that in Figure 4c. Since no condition has been changed except for the solution pH, we deduce that further increasing of pH does not favor

(16) Hu, X.-L.; Zhu, Y.-J. *Chem. Lett.* **2004**, *33*, 880−881.
(17) Garvie, R. C.; Nicholson, P. S. *J. Am. Ceram. Soc.***1972**, *55*, 303−305.

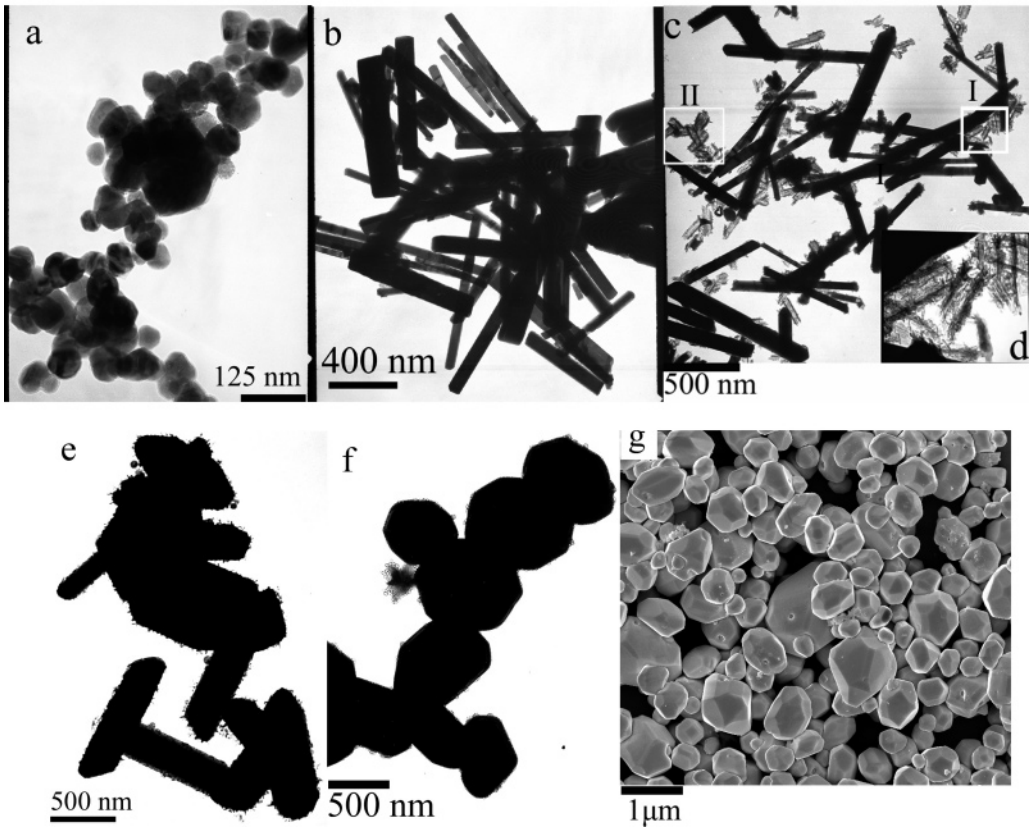

Figure 4. Typical TEM images of Pb-based chromate sample synthesized without surfactant under various pH conditions: (a) pH 1; (b) pH 4; (c, d) pH 7; (e) pH 9; (f) pH 14. (g) Typical SEM image of the sample synthesized at pH 14.

the formation of nanorods and pH 7 might be the optimal condition for the formation of such rodlike structures. The conclusion is further evidenced as the pH is increased continuously. When the pH is increased to 14, the pure phase of Pb_2CrO_5 can only be seen (JCPDS: 84-0678) and $PbCrO_4$ disappears (Figure 3e). Accordingly, the rodlike structure vanishes (Figure 4f−g).

To explain the formation of 1D nanostructures, the spherical diffusion model and the cylindrical diffusion model were proposed in previous literature.[18] These models indicate that the varied solution concentration will change the chemical potential of the crystal faces and lead to anisotropic lateral growth of the crystals. In the present work, the concentration of $[CrO_4^{2-}]$, on the basis of the equilibrium equation of $Cr_2O_7^{2-} + H_2O \rightleftharpoons 2CrO_4^{2-} + 2H^+$, will be changed under a different pH. However, it is difficult to explain the formation of 1D nanocrystals of chromate completely via the above model because of phase transformation along with change of pH. We expect the full explanation will be given by our following work soon.

Effect of pH on the Synthesis of Ba-Based Chromate Nanorods. The effects of pH on the formation of rodlike structures are further evidenced in the preparation of barium chromate nanorods. Under pH 7, $BaCrO_4$ nanorods have been successfully obtained and the morphology percent is 100. As the pH is increased to 14, only the particle-like structure

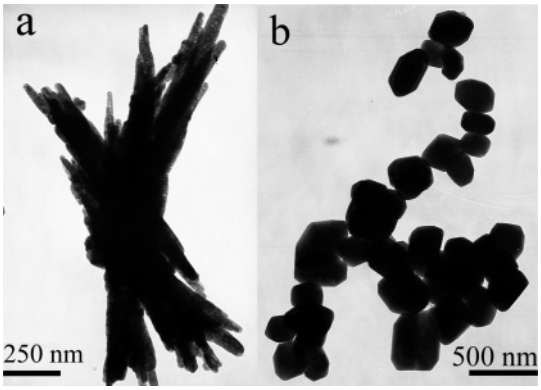

Figure 5. Typical TEM images of Ba-based chromate sample synthesized without surfactant under various pH conditions: (a) pH 7; (b) pH 14.

is obtained and the rodlike structure disappears (morphology percent is 0). The corresponding TEM images are shown in Figure 5a,b. The XRD patterns of as-synthesized chromate samples under different conditions are shown in Figure 6. It is shown that the sample is poorly crystalline in Figure 6a. The samples corresponding to Figure 6b,c are well crystallized, and both reflections are easily indexed to an orthorhombic type structure (space group *Pnma* (No. 62)) and lattice constants $a = 9.113$ Å, $b = 5.528$ Å, $c = 7.336$ Å, and $\alpha = \beta = \gamma = 90°$ (JCPDS: 78-1401).

Effect of pH on the Synthesis of Cu-Based Chromate Nanostructures. On the basis of the previous literature, coprecipitation of $[Cu^{2+}]$ and $[CrO_4^{2-}]$ is highly sensitive to initial pH and $CuCrO_4$ products can be produced at pH 5.0−5.2.[19] However, pure $CuCrO_4$ phase has not been obtained

(18) (a) Sugimoto, T. *Photogr. Sci. Eng.* **1989**, *28*, 137. (b) Sugimoto, T. *J. Imaging Sci.* **1989**, *33*, 203. (c) Karpinski, P. H.; Wey, J. S. *J. Imaging Sci.* **1988**, *32*, 34.

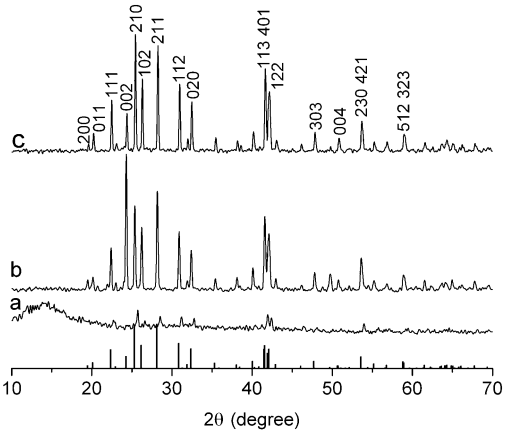

Figure 6. Typical XRD patterns of $BaCrO_4$ under different solution conditions via the hydrothermal method in the absence of surfactant: (a) pH 5; (b) pH 7; (c) pH 14. The histogram, just at the bottom of the XRD patterns, shows the calculated powder diffraction pattern arising from JCPDS 78-1401.

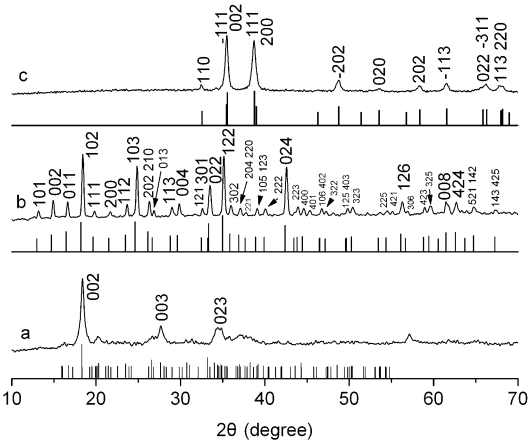

Figure 7. Typical XRD patterns of Cu-based chromate compounds under different solution conditions via the hydrothermal method in the absence of surfactant: (a) pH 5; (b) pH 11; (c) pH 14. The histogram, just below the XRD pattern, shows the calculated powder diffraction pattern arising from (a) JCPDS 38-231, (b) JCPDS 39-0051, and (c) JCPDS 80-1268, respectively.

at pH 5 in this work. The XRD pattern of the synthesized sample is shown in Figure 7a, which is poorly crystallized and partly indexed to triclinic $Cu(OH)_{14}(CrO_4)_4$ (JCPDS: 38-231). The reason is that once the precipitation of $CuCrO_4$ is produced at pH 5, the solution will become heterogeneous, which will lead to subsequent formation of other type precipitates such as copper hydroxide chromate precipitate (xCuCrO$_4$·yCu(OH)$_2$). The production of multiple precipitated species in the present reaction system will cause difficulties to prepare the Cu−Cr precipitates with a precise stoichiometry.[19] However, when pH is further increased to 11, pure copper chromate hydroxide precipitate will be produced. The XRD pattern of the as-synthesized sample is shown in Figure 7b. The formula of the product is $CuCrO_4$·$2Cu(OH)_2$·$2H_2O$ (or Cu_3CrO_6·$2H_2O$). All the reflections of Figure 7b are easily indexed to an orthorhombic type (space group: *Pnma* (No. 2)) with lattice constants $a = 8.262$ Å, $b = 6.027$ Å, $c = 12.05$ Å, and $\alpha = \beta = \gamma = 90°$ (JCPDS: 39-0051). As the pH is increased to 14, the final product is CuO and the XRD patterns of as-produced CuO are well indexed to a monoclinic type (space group $C2/c$ (No. 15)) with lattice constants $a = 4.683$ Å, $b = 3.421$ Å, $c = 5.129$ Å, and $\beta = 99.57°$ (JCPDS: 80-1268). The reason is that, at high pH, $Cu(OH)_2$ can be produced instead of copper chromate hydroxide (xCuCrO$_4$·yCu(OH)$_2$) due to its extremely small solubility product constant ($k_{sp} = 1.3 \times 10^{-20}$). $Cu(OH)_2$ will decompose to CuO when the sample is heated. The morphologies of $CuCrO_4$·$2Cu(OH)_2$·$2H_2O$ and CuO samples comprise all beltlike structures.

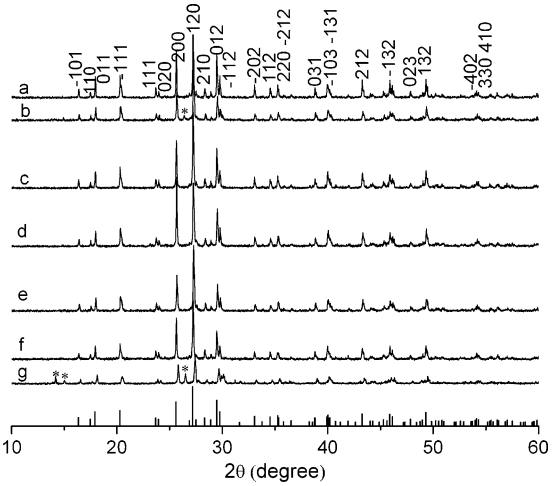

Figure 8. XRD patterns of $PbCrO_4$ nanorods synthesized with various surfactants at initial solution pH 7: (a) PVP; (b) PEG; (c) PVA; (d) stearylamine; (e) stearinic acid; (f) CTAB; (g) SDS. (An asterisk denotes an impurity of the Pb_2CrO_5 phase.) The samples are synthesized at 140 °C for 20 h, pH 7. The histogram, just at the bottom of the XRD patterns, shows the calculated powder diffraction pattern arising from JCPDS 73-2059.

Effect of Surfactant on the Formation of Chromate Nanorods/Nanobelts. The Pb-based chromate sample has been chosen to study the effect of surfactant on the formation of chromate nanorods/nanobelts. XRD patterns of $PbCrO_4$ nanorods synthesized with various surfactants (1 wt %) are shown in Figure 8.

The weight percent (1 wt %) of surfactant is the ratio of the weight of surfactant added into the reaction to the general weights of all the inorganic precursors (shown in column 1 in Table 1). It can be shown that almost all of the products is pure $PbCrO_4$ phase. There are very few Pb_2CrO_5 phases (marked by an asterisk) in the products for Figure 8b,g. All the products are fabricated in the presence of surfactants (1 wt %) of PVP (poly(vinyl pyrrolidone)) (Figure 8a), PEG (poly(ethylene glycol)) (Figure 8b), PVA (poly(vinyl alcohol)) (Figure 8c), stearylamine (Figure 8d), stearinic acid (Figure 8e), CTAB (cetyltrimethylammonium bromide) (Figure 8f), and SDS (sodium dodecyl sulfate) (Figure 8g), respectively. The reflections of pure phase $PbCrO_4$ are all indexed to a monoclinic type (JCPDS: 73-2059). Some typical SEM images of the above as-synthesized $PbCrO_4$ samples are shown in Figure 9.

As discussed previously, under the conditions of 140 °C, 20 h, in the absence of surfactants, pure $PbCrO_4$ phase will be produced at initial pH 1 and the mixture of the $PbCrO_4$

(19) Sun, J.-M.; Shang, C.; Huang, J.-C. *Environ. Sci. Technol.* **2003**, *37*, 4281−4287.

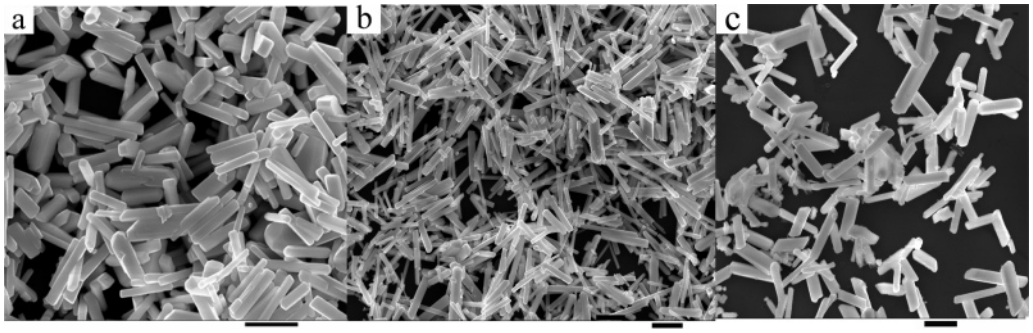

Figure 9. Typical SEM images of $PbCrO_4$ nanorods in the presence of surfactants of (a) PVA, (b) PEG, and (c) stearinic acid (bar: 1 μm).

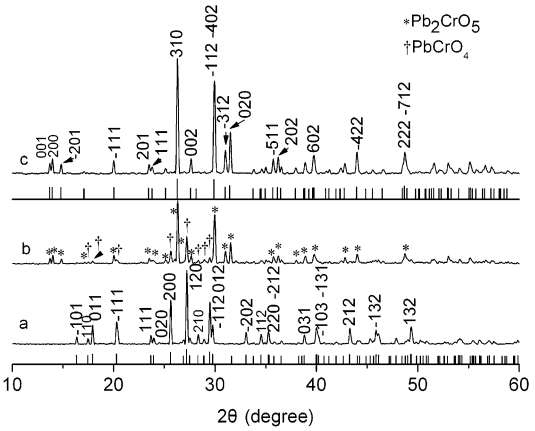

Figure 10. XRD patterns of Pb-based chromates synthesized in the presence of surfactant of PVP at initial solution pH (a) 7, (b) 14, and (c) $[OH^-] = 2.0$ mol·L^{-1}. The histogram, just below the XRD pattern, shows the calculated powder diffraction pattern arising from (a) JCPDS 73-2059 and (c) JCPDS 84-0678, respectively. On the basis of eq 3, the phase content of $PbCrO_4$ is (a) 100%, (b) 28.1%, and (c) 0, respectively.

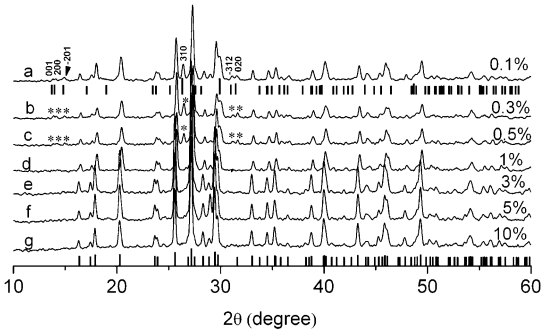

Figure 11. XRD patterns of Pb-based chromates synthesized with varied weight percent of PVP at initial solution pH 7: (a) 0.1 wt %; (b) 0.3 wt %; (c) 0.5 wt %; (d) 1 wt %; (e) 3 wt %; (f) 5 wt %; (g) 10 wt %. The histogram, just below (a), shows the calculated powder diffraction pattern of Pb_2CrO_5 arising from JCPDS 84-0678, and the histogram, just below (g), shows the calculated powder diffraction pattern of $PbCrO_4$ arising from JCPDS 73-2059. (The asterisk refers to the Pb_2CrO_5 phase.) On the basis of eq 3, the phase content of $PbCrO_4$ is (a) 78.5%, (b) 79.1%, (c) 80.1%, (d) 100%, (e) 100%, (f) 100%, and (g) 100%, respectively.

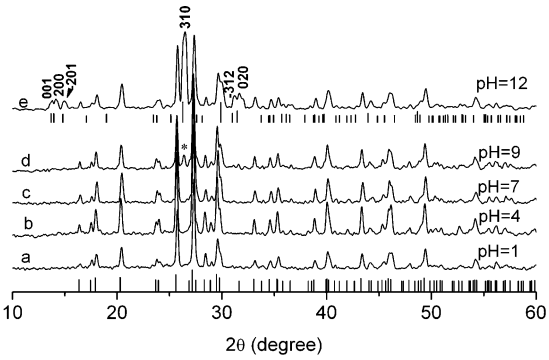

Figure 12. XRD patterns of Pb-based chromates synthesized at varied initial solution pH with 1 wt % PVP: (a) pH 1; (b) pH 4; (c) pH 7; (d) pH 9; (e) pH 12. The histogram, just below (a), shows the calculated powder diffraction pattern of $PbCrO_4$ arising from JCPDS 73-2059, and the histogram, just below (e), shows the calculated powder diffraction pattern of Pb_2CrO_5 arising from JCPDS 84-0678. (The asterisk refers to the Pb_2CrO_5 phase.) On the basis of eq 3, the phase content of $PbCrO_4$ is (a) 100%, (b) 100%, (c) 100%, (d) 82.9%, and (e) 62.1%, respectively.

and Pb_2CrO_5 phases will be produced at initial pH 7 (Figure 3a,c). However, in the presence of surfactants, pure $PbCrO_4$ phase will also be prepared under the conditions of the same temperature (140 °C) and the same reaction time (20 h) and initial pH 7 (Figure 8). The reasonable explanation for the formation of pure $PbCrO_4$ phase at pH 7 in the presence of surfactants is that the added surfactants could enclose local regions of lower pH, which offer a favorable environment for the crystal growth of pure lead chromate.

To explain the phenomenon expressly, contrast experiments are carried out under initial pH 14 and $[OH^-] = 2.0$ mol·L^{-1} in the presence of surfactant with other reaction conditions unchanged. The added surfactant is PVP with 1 wt %. The XRD patterns of the products are shown in Figure 10.

As shown in Figure 10, the mixture phases of $PbCrO_4$ and Pb_2CrO_5 are produced under pH 14 in the presence of surfactant (Figure 10b) instead of pure Pb_2CrO_5 phase under the same pH condition in the absence of surfactant (Figure 3e). The pure Pb_2CrO_5 phase can be produced under $[OH^-] = 2.0$ mol·L^{-1} (Figure 10c) in the presence of surfactant (PVP). The facts shown in Figure 10 confirm the judgments that the added surfactant will enclose local regions of lower pH in the environment for the crystal growth of chromates.

To further confirm the conclusion, more control experiments have been made. In the control experiments, PVP (poly(vinyl pyrrolidone)) has also been chosen to be a typical surfactant for the research. Compared with 1 wt % and pH 7, two parallel tests have been made. One is that weight percents of 0.1, 0.3, 0.5, 3, 5, and 10 have been chosen to contrast with 1% at fixed initial solution pH 7 (Figure 11), and the second is that pH values 1, 4, 9, and 12 have been chosen to contrast with 7 with fixed weight percent of 1% of PVP (Figure 12). From Figure 11, it is obvious that, at fixed pH 7, no impurity phase of Pb_2CrO_5 will be observed when the weight percent of PVP is larger than 1, which

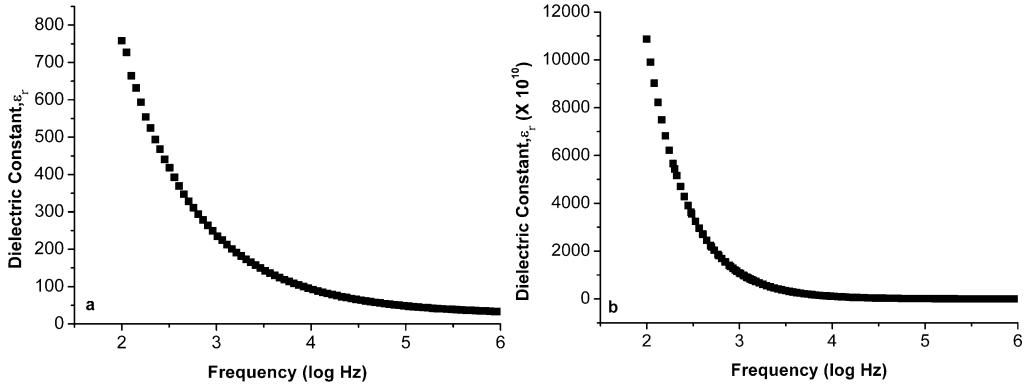

Figure 13. Variation of dielectric constants of (a) $PbCrO_4$ nanorods and (b) $CuCrO_4$ nanobelts, as a function of denary logarithm of frequency.

reveals that in exceeding 1 wt % of PVP in the local regions enclosed with surfactant favors growth of pure lead chromate. To demonstrate the results clearly, the reflections of (001), (200), ($\bar{2}$01), (310), ($\bar{3}$12), and (020) of Pb_2CrO_5 have been indexed in Figure 11a. In Figure 11b,c, the asterisk is referred to the Pb_2CrO_5 phase.

For Figure 12, it is visible that with fixed 1 wt % PVP, pure $PbCrO_4$ can be obtained when the pH is smaller than 7, and to demonstrate the results clearly, the reflections of (001), (200), ($\bar{2}$01), (310), ($\bar{3}$12), and (020) of Pb_2CrO_5 have been indexed in Figure 12e. In Figure 11d, the asterisk is referred to the Pb_2CrO_5 phase.

The above conclusion is also consisted with the synthesis of Cu-based chromate. Pure $CuCrO_4$ will be produced at pH 7 in the presence of surfactant of PVP, whereas $CuCrO_4$ can be produced at pH 5.0−5.2 in the absence of surfactant in the previous literature.[19]

According to the careful analyses and comparisons with the above facts, we hypothesize that the reason for the added surfactant is it favors formation of as-synthesized lead chromate crystal. When the surfactants are added to the solution, long chains of the surfactants form a nanoreactor. The topologies of these nanoreactors can be spherical, wormlike, etc., according to different water/surfactant ratios. The nanoreactor thus can be used as a soft template to control the morphology of inorganic materials synthesized in it. As the phase transform in the current case, the nanoreactor might enclose local regions of lower pH, which offer a favorable environment for the crystal growth of as-synthesized lead chromate. It should be noted that crystal growth is a complex process, which is related to thermodynamics, dynamics, and environments for crystal growth. Thus, it is a difficult and complicated process to understand the mechanism of crystal growth. In the present time, our knowledge about the mechanism of the effects of surfactants has been comparatively superficial and further understanding for the mechanism needs much more work. It is hoped that we can achieve this in the coming time.

Dielectric Properties of As-Synthesized Chromate Nanorods/Nanobelts. The dielectric constant can be obtained by $\epsilon_r = (t_a c_p)/(\pi r^2 \epsilon_0)$, where t_a is the thickness of the sample, 1.23 mm, r is the measured radius of the disc-shaped specimen, 4.67 mm, ϵ_0 is the dielectric constant in air, 8.854 $\times$ 10^{-12} F/m, and c_p is the measured capacitance.[20] The measurement has been made with the impedance analyzer (HP4194A) at room temperature. The corresponding results, the variation of dielectric constant as a function of denary logarithm of frequency for $PbCrO_4$ nanorods and $CuCrO_4$ nanobelts, are shown in Figures 11a and 13b, respectively.

It is obvious from Figure 13 that the dielectric constant decreases with increasing frequency. The decline velocity is much less at the frequency of 10^3 Hz and becomes constant with higher frequencies. The detected dielectric results shown in Figure 13a,b are not quite the same. The dielectric constant of $PbCrO_4$ nanorods is comparatively high. However, the value of $CuCrO_4$ nanobelts is very small. The difference may be explained by using interfacial polarizability. A specified component of polarizability characterizes the polarization of dielectrics. The meaning of interfacial polarizability is that in a real crystal there inevitably exist a large number of defects such as lattice vacancies, impurity centers, dislocations, and so on. Free charge carriers, migrating through the crystal under the influence of an applied field, may be trapped by, or pile up against, a defect. The effect of this will be the creation of a localized accumulation of charge and give rise to a dipole moment and constitutes a separate mechanism of polarization in the crystal, which is referred to as interfacial polarizability. It is known that different crystals will hold different interfacial polarizabilities in the given condition, which may account for the discriminating dielectric characteristics of $PbCrO_4$ and $CuCrO_4$ crystals shown in Figure 13a,b.[21] High permittivity of $PbCrO_4$ nanorods in the lower frequency, the maximum value is about 800, mainly arises from the interfacial polarization, formed with the accumulations of the charges, at the surfaces of $PbCrO_4$ nanorods. The accumulations of the charges require some time, and when the processes of accumulations cannot follow the variations of applied fields, the mechanism of interfacial polarization may not make a contribution to the dielectric constant. Then the apparent permittivity will fall to low value with increasing frequency. The high permittivity may offer the possibility of capacitors having large capacitance combined with small size. A further advantage of the small

(20) Nair, K. M., Bhalla, A. S., Eds. *Dielectric ceramic materials*; The American Ceramic Society: Westerville. OH, 1999; p 133 (ISBN 1-57498-066-1).
(21) Anderson, J. C., Ed. *Dielectrics*; first published by Chapman and Hall Ltd.: London, 1964; pp 41−49, 52.

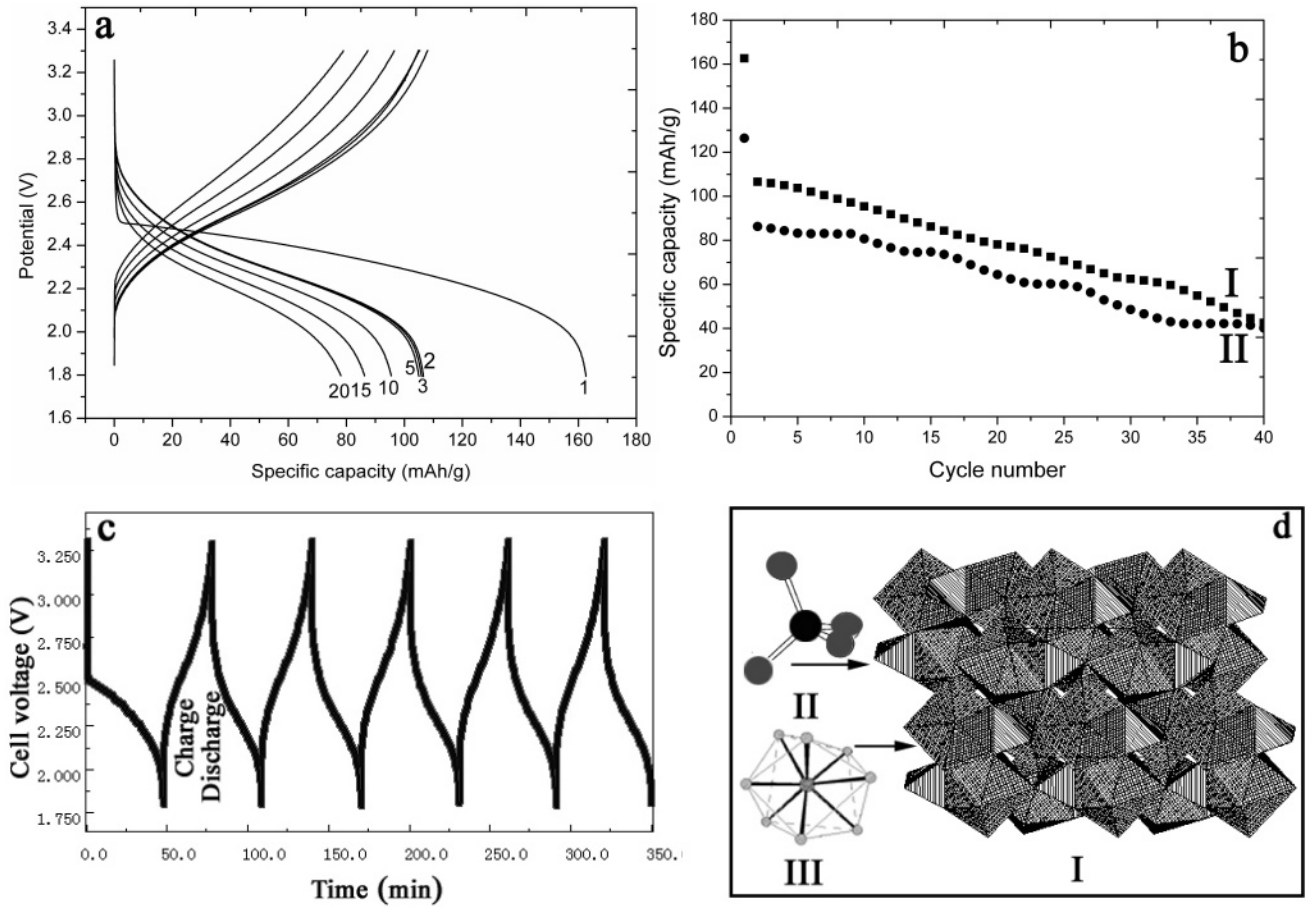

Figure 14. (a) Several charge (top) and discharge (bottom) curves, (b) cycling behavior, and (c) charging and discharging voltage plotted versus cycle time of $PbCrO_4$/Li cells using nanorods as a cathode (positive electrode) and lithium as an anode (negative electrode) in the voltage 1.8−3.3 V, where the constant currents used were ±0.2 mA. The entire cell test was carried out at room temperature, and the current density (CD) of the active cathode materials was 0.2 mA mg^{-1}. For comparison the data in (b) II of the cell were measured while the current density (CD) was 0.05 mA mg^{-1}. (d) Crystal structure of $PbCrO_4$ materials.

capacitor is that it can readily be built into a programmer in which resistors, connecting wires, and transistors are produced by vacuum depositions. These "integrated circuits" are at present being actively developed and are of considerable potential importance.[22]

The dielectric constant of $CuCrO_4$ nanobelts is very small as shown in Figure 13b; the maximum value is only about 1.0×10^{-7}, which is due to the high conductivity itself. The small permittivity shows that the $CuCrO_4$ nanocrystal is not a good dielectric material; however, it is expected that $CuCrO_4$ nanobelts can be potentially used as good semiconductors.[23]

Electrochemical Properties of As-Synthesized Chromate Nanorods/Nanobelts. The electrochemical properties of the $PbCrO_4$ nanorods as electrode materials for Li-based batteries were characterized in the voltage range 1.8−3.3 V versus Li^+/Li at a constant current of ±0.2 mA. A high capacity of 163 mA h g^{-1} was obtained in the first discharge process (Figure 14a). This corresponds to the insertion of ca. 1.97 lithium/unit of $PbCrO_4$. Similar to other Li-storage nanoscale materials,[24] the $PbCrO_4$ nanorods also present a considerable capacity loss (56 mA h g^{-1}) during the second cycle. However, the materials subsequently exhibited excellent cyclability with an average capacity loss ratio ~1.5%/cycle (Figure 14 (I)). Figure 14c shows the voltage profile vs time of the cell during the discharging and during the next few charge−discharge cycles, and it is clear that the cell displays excellent reversibility. The cell was discharged (Li inserted) to 1.8 V and charged (Li released) to 3.3 V. Data in Figure 14c were extracted for the first six cycles; the nice reversibility indicates that the $PbCrO_4$ nanocrystal can act as a potential good alternative electrode material for a Li-based rechargeable battery in the future.[25] The crystal structure of $PbCrO_4$ nanorods is shown in Figure 14d, and I is the polyhedral packing structure for this crystal. It is indicated that the polyhedral structure is built-up with a CrO_4 tetrahedron (Figure 14d (II)) and PbO_8 square antiprism (Figure 14d (III)). In the CrO_4 tetrahedron, Cr^{6+} takes up the central position and four O^{2-} ions hold the positions in the four vertex corners. In the PbO_8 group, the central position is occupied with a Pb^{2+} cation, which is surrounded

(22) (a) Yun, W. S.; Urban, J. J.; Gu, Q.; Park, H. K. *Nano Lett.* **2002**, *2*, 447−450. (b) Kim, L.; Jung, D. *Appl. Phys. Lett.* **2003**, *82*, 2118.
(23) Gu, B. L.; Wang, X. K. *Solid-state physics*; Tsinghua University Press: Tsinghua, P. R. China, 1990.
(24) Ma, R. Z.; Bando, Y.; Zhang, L. Q.; Sasaki, T. *Adv. Mater.* **2004**, *16*, 918−922.
(25) Idota, Y.; Kubota, T.; Matsufuji, A.; Maekawa, Y.; Miyasaka, T. *Science* **1997**, *276*, 1395−1397.

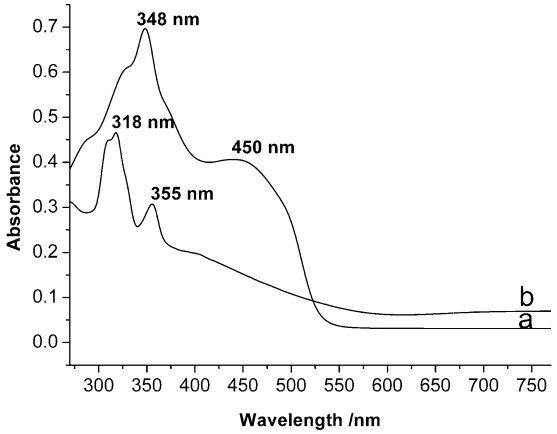

Figure 15. UV−vis absorption spectra of (a) $PbCrO_4$ nanorods and (b) $CuCrO_4$ nanobelts.

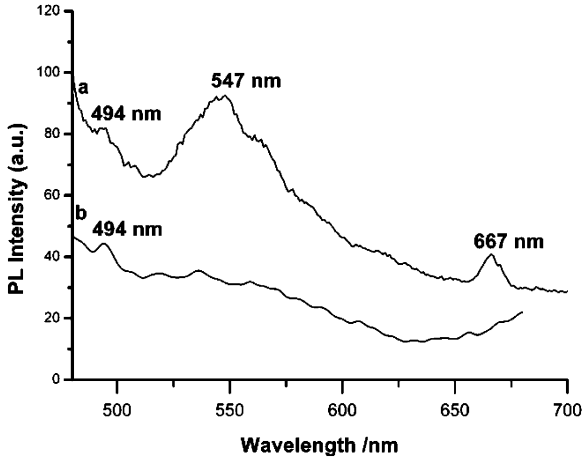

Figure 16. PL spectra of as-synthesized samples of (a) $PbCrO_4$ nanorods and (b) $CuCrO_4$ nanobelts. The excitation wavelength in (a) is 445 nm and in (b) is 350 nm.

by eight O^{2-} anions to form a square antiprism. It is shown that $PbCrO_4$ does not have a layered, spinel, or olivine structure such as the common electrode materials for Li-based rechargeable batteries.[26] Hence, the mechanism of the reaction of lithium with $PbCrO_4$ differs from the classical lithium insertion/deinsertion or lithium-alloying processes. As reported by Tarascon's group,[27] the difference is due to the facts that the structure of most corresponding materials does not contain any available sites for Li ions (for instance $PbCrO_4$ as shown in Figure 14d) and also that these materials cannot form alloys with lithium. Thus concerning the present reversible electrochemical reaction of Li with $PbCrO_4$ materials, the mechanism may involve the formation and decomposition of Li_2O, accompanying the redox reactions. Although Li_2O and other metal oxides have been regarded as electrochemical inactive materials at room temperature, the size of the particles is believed to enhance their electrochemical activity in the above process. Hence, a reversible electrochemical reaction may occur.[27,28]

Optical Properties of As-Synthesized Chromate Nanorods/Nanobelts. The diffusive reflectance spectra of the as-synthesized chromates nanorods/nanobelts are shown in Figure 15. The Kubelka−Munk Function,[29] which is the ratio between the absorption and scattering factors, is then used for the absorbance plotting. As shown in Figure 15, the peak of the absorption pattern is around at 348 nm (Figure 13a) and 318 nm (Figure 15b), respectively.

In the unit cell of chromate, Cr^{6+} and O^{2-} ions form the CrO_4 tetrahedron, in which the four vertex corners are occupied by O^{2-} ions and the central position is occupied by a Cr^{6+} ion (Figure 14d (II)). The band structures of chromate are generally defined by the Cr-3d level and O-2p level when the d orbitals of chromium atom are empty.[30] Hence, it is suggested the conduction bands of $PbCrO_4$ and $CuCrO_4$ are composed of the Cr^{6+} 3d orbital, and the valence bands are composed of the O 2p orbital. The maximal optical absorptions around 348 nm for $PbCrO_4$ nanorods (Figure 15a) and 318 nm for $CuCrO_4$ nanobelts (Figure 15b) may be ascribed to the electronic excitation from the O 2p state to the Cr^{6+} 4s state or Cu^{2+} 3d state or Pb^{2+} 6p state.[30]

The photoluminescence (PL) properties of as-synthesized samples are also investigated. As shown in Figure 16a, $PbCrO_4$ nanorods display emission properties with three characteristic peaks centered at 494 nm (2.51 eV), 547 nm (2.27 eV), and 667 nm (1.86 eV), respectively, which are excited at about 445 nm (2.79 eV). The PL spectrum of $CuCrO_4$ nanobelts is shown in Figure 16b, and it is observed that there are no emission properties except for a very weak peak centered at about 494 nm (2.51 eV) when excited at 350 nm (3.54 eV). Such very slight emission peak centered at 494 nm (2.51 eV) appearing in Figure 16a,b might be ascribed to the $[CrO_4^{2-}]$ complex anion of slightly distorted tetrahedral symmetry probably induced by the Jahn−Teller effect.[31] The PL peaks centered at 547 nm (2.27 eV) and 667 nm (1.86 eV) shown in Figure 16a may be attributed to the energy emission from the Pb^{2+} 6s state to lower energy state. The reason there is no emission peak behind the 500 nm wavelengths in Figure 16b is that the ion of Cu^{2+} has 9 electrons in its 3d shell and the shell of 3d will be filled when an electron is excited from the O 2p state into the Cu $3d^9$ state. The electrons in the full $3d^{10}$ are in the energy-stable state, and they are difficult to transfer into a lower energy level. These investigations are in progress, and further study will be needed.

Conclusions

In the current contributions, a facile, robust, and low-cost solution-based hydrothermal general synthesis method is introduced to prepare a family of chromate 1D nanostructures. The current method can be used to fabricate a family of chromate nanostructures, such as $PbCrO_4$, $CuCrO_4$,

(26) Thackeray, M. *Nat. Mater.* **2002**, *1*, 81−82.
(27) Poizot, P.; Laruelle, S.; Grugeon, S.; Dupont, L.; Tarascon, J.-M. *Nature* **2000**, *407*, 496.
(28) Li, H.; Richter, G.; Maier, J. *Adv. Mater.* **2003**, *15*, 736−739.
(29) Kortüm, G. *Reflectance Spectroscopy: Principles, Methods, Applications*; Springer-Verlag: Berlin, Heidelberg, Germany, 1969.
(30) (a) Yin, J.; Zou, Z.; Ye, J. *Chem. Phys. Lett.* **2003**, *378*, 24−28. (b) Aoki, Y.; Konno, H. *J. Solid State Chem.* **2001**, *156*, 370−378.
(31) (a) Springis, M.; Tale, V.; Tale, I. *J. Lumin.* **1994**, *72*−*74*, 784−785. (b) Nikl, M.; Strakova, P.; Nitsch, K.; Petrýcek, V.; Mucka, V.; Jarolýmek, O.; Novak, J.; Fabeni, P. *Chem. Phys. Lett.* **1998**, *291*, 300−304.

$SrCrO_4$, $CaCrO_4$, $BaCrO_4$, $4ZnCrO_4{\cdot}K_2O{\cdot}3H_2O$, $NiCrO_4$, amd Ag_2CrO_4. The effects of solution pH and surfactants are also investigated. It is shown that pH 7 is the optimal condition for the formation of chromate 1D nanostructures and surfactants added into the solution will lowered the pH in the reaction solution. The physical properties, such as dielectric, electrochemical, UV−vis absorbance, and photoluminescent properties, of the as-synthesized chromate nanocrystals have also been studied.

In the future, we will extend our approach toward the synthesis of other metal transition 1D oxysalts nanostructures.

Acknowledgment. This work was supported by the NSFC (Grants 90406003, 20401010, 50372030, 20025102, 20131030), the Foundation for the Author of National Excellent Doctoral Dissertation of P. R. China, and the State Key Project of Fundamental Research for Nanomaterials and Nanostructures (Grant 2003CB716901).

Supporting Information Available: XRD patterns and TEM images of other chromate nanorods/nanobelts. This material is available free of charge via the Internet at http://pubs.acs.org.

IC048237+